Preprints of the 21st IFAC World Congress (Virtual)
Berlin, Germany, July 12-17, 2020

Observer of Coupled Hyperbolic PDEs for Deep-sea Construction Vessel Vibrations

Ji Wang and Miroslav Krstic

Department of Mechanical and Aerospace Engineering, University of California, San Diego, La Jolla, CA 92093-0411, USA

Abstract: Motivated by vibration state estimation of a deep-sea construction vessel used to install oil drilling equipment on the seafloor, this paper presents state observer design of a 4×4 coupled heterodirectional hyperbolic PDE-ODE system, characterized by spatially-varying coefficients and a time-varying domain. The exponential stability of the observer error system is proved via Lyapunov analysis. Effective estimation of lateral-longitudinal coupled vibration states of the deep-sea construction vessel is verified in numerical simulation.

Keywords: Distributed parameter system, Hyperbolic PDEs, Observer design, Deep-sea construction vessel.

1. INTRODUCTION

In deep-sea oil exploration, a deep-sea construction vessel (DCV) shown in Fig. 1 is an important device used to install equipment such as a subsea manifold, a subsea pump station, flowlines and so on, at the designated locations around the drill center on the seafloor Stensgaard et al. (2010); Standing et al. (2002). A dominant component in the DCV is a long cable with time-varying length, of which the top is attached to a ship-mounted crane and the bottom is attached to the equipment (referred to as payloads hereafter). Undesired vibration is usually easy to be aroused in such a compliant cable system Wang el al. (2018a), and a real-time vibration estimator of the distributed vibrations in cable is helpful for designing boundary vibration control strategies of DCV where the distributed vibration states along cable are unmeasurable.

According to the dynamic modelling of DCV in Wang et al. (2019a), two-dimensional vibrations of DCV can be described by a coupled wave PDE model. Therefore, the vibration estimator design of DCV requires developing state-observer design of a class of wave PDE model. It is a good way to reduce the order of PDEs by introducing Riemann transformations to convert the plant to coupled transport PDEs Roman et al. (2019); Wang el al. (2020). Observer design for such a coupled transport PDE system can be found in Hu et al. (2016); Anfinsen et al. (2017a,b); Deutscher (2017b); Deutscher et al. (2019); Deutscher (2017a). However, the above works focus on coupled transport PDEs on a constant domain while the PDE model of DCV is on a time-varying domain because of the cable of time-varying length. An observer for 2×2 coupled transport PDEs on a time-varying domain was proposed in Wang el al. (2018b) where only one-dimensional vibration is considered. In this paper, we propose a state observer for a 4×4 coupled transport PDEs on a time-varying domain with application of two-dimensional vibration estimation for DCV, where only a two-direction accelerometer at the ship-mounted crane is used.

This paper is organized as follows. The concern plant is described in Section 2. A state observer is designed in Section 3 and the exponential convergence to zero of observer errors

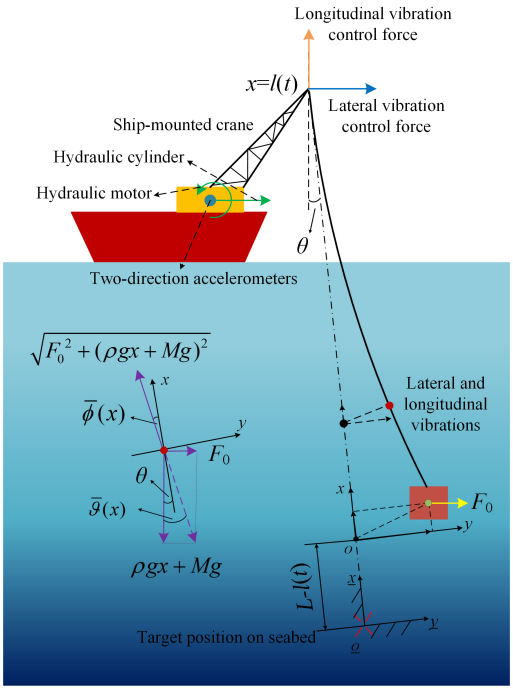

Fig. 1. Deep-sea Construction Vessel.

is proved in Section 4. In Section 5, the theoretical result is applied in the specific model of the DCV and the performance on vibration estimation of DCV is tested. In Section 6, the conclusion is provided.

2. PROBLEM FORMULATION

The concern plant, i.e., a general form of the two-dimensional vibrations of the deep-sea construction vessel (DCV) derived in Section II.B in Wang et al. (2019a), is

$$\begin{aligned} w_{tt}(x,t) &= d_1(x)w_{xx}(x,t)+d_2(x)w_x(x,t)+d_3(x)u_x(x,t) \\ &\quad +d_4(x)w_t(x,t)+d_5(x)u_t(x,t), \qquad (1) \\ u_{tt}(x,t) &= d_6(x)u_{xx}(x,t)+d_7(x)w_x(x,t)+d_8(x)u_x(x,t) \\ &\quad +d_9(x)w_t(x,t)+d_{10}(x)u_t(x,t), \qquad (2) \end{aligned}$$

$$w_{tt}(0,t) = d_{11}w_t(0,t) + d_{12}w_x(0,t) + d_{13}u_t(0,t) + d_{14}u_x(0,t), \quad (3)$$

$$u_{tt}(0,t) = d_{15}u_t(0,t) + d_{16}u_x(0,t) + d_{17}w_t(0,t) + d_{18}w_x(0,t), \quad (4)$$

$$u_x(l(t),t) = d_{19}(l(t))U_1(t), \quad (5)$$

$$w_x(l(t),t) = d_{20}(l(t))U_2(t), \quad (6)$$

$\forall (x,t) \in [0, l(t)] \times [0,\infty)$. Wave PDEs w and u are coupled with each other both in the domain and at the dynamic boundary, which can physically describe longitudinal-lateral coupled vibrations. Control inputs $U_1(t), U_2(t)$ designed here are related to longitudinal and lateral control forces provided by the hydraulic motor and cylinder at the ship in practice. The assumed measurements are $u_t(l(t),t), w_t(l(t),t)$. Note that in practice, the available measurements actually are acceleration signals $u_{tt}(l(t),t), w_{tt}(l(t),t)$ obtained by accelerometers placed at the crane, because measuring vibrational acceleration rather than velocity/displacement is a more convenient way in vibrational mechanical system. The velocity signals $u_t(l(t),t), w_t(l(t),t)$ can then be obtained by integrations of the measured acceleration signals under known initial conditions.

System coefficients d_{12}, d_{11}, d_{13}, d_{16}, d_{17}, d_{15}, d_{18}, d_{14} are arbitrary constants and $d_{19}(l(t)), d_{20}(l(t))$ are nonzero. The time-varying domain, i.e., moving boundary $l(t)$ and the spatially-varying coefficients $d_1(x)$, $d_2(x)$, $d_3(x)$, $d_6(x)$, $d_7(x)$, $d_8(x)$, $d_4(x), d_5(x), d_9(x), d_{10}(x)$ are under the following assumptions:

Assumption 1. $l(t)$ is bounded by $0 < l(t) \leq L, \forall t \geq 0$.

Assumption 2. $\dot{l}(t)$ is bounded by $[\underline{M}, \overline{M}]$, where $\overline{M}$ satisfies $\overline{M} < \min_{0\leq x\leq L}\{\sqrt{d_1(x)}, \sqrt{d_6(x)}\}$, and $\underline{M}$ is arbitrary in $(-\infty, \overline{M})$.

Assumption 3. The spatially-varying coefficients $d_1(x)$, $d_2(x)$, $d_3(x), d_4(x), d_5(x), d_6(x), d_7(x), d_8(x), d_9(x), d_{10}(x)$ are bounded, $\forall x \in [0, L]$.

Assumption 4. $d_1(x), d_6(x) \in C^1$ are positive and $d_1(x) \neq d_6(x)$, $\forall x \in [0, L]$.

Remark 1. Assumptions 1-4 about the spatially-varying coefficients and the time-varying spatial domain of (1)-(6) are fully satisfied in the application of the DCV, which can be easily checked by the specific expressions of $d_1, \ldots, d_{20}$ (84)-(90) and parameter values in Tab. 1 of the DCV in the simulation.

3. OBSERVER DESIGN

3.1 Reformulation of the plant (1)-(6)

The observer design would be conducted based on a equivalent reformulated system where the PDE order is reduced by introducing Riemann transformations:

$$z(x,t) = w_t(x,t) + \sqrt{d_1(x)}w_x(x,t), \quad (7)$$

$$v(x,t) = w_t(x,t) - \sqrt{d_1(x)}w_x(x,t), \quad (8)$$

$$k(x,t) = u_t(x,t) + \sqrt{d_6(x)}u_x(x,t), \quad (9)$$

$$y(x,t) = u_t(x,t) - \sqrt{d_6(x)}u_x(x,t). \quad (10)$$

Defining

$$X(t) = [w(0,t), w_t(0,t)], \;\; Y(t) = [u(0,t), u_t(0,t)], \quad (11)$$

and

$$p(x,t) = [y(x,t), v(x,t)]^T, \quad (12)$$

$$r(x,t) = [k(x,t), z(x,t)]^T, \quad (13)$$

$$W(t) = [X(t), Y(t)]^T, \quad (14)$$

(1)-(6) can be reformulated as

$$p_t(x,t) + Q(x)p_x(x,t) = T_a(x)r(x,t) + T_b(x)p(x,t), \quad (15)$$

$$r_t(x,t) - Q(x)r_x(x,t) = T_a(x)r(x,t) + T_b(x)p(x,t), \quad (16)$$

$$p(0,t) = C_3W(t) - r(0,t), \quad (17)$$

$$\dot{W}(t) = (\bar{A} - \bar{B}C_3)W(t) + 2\bar{B}r(0,t), \quad (18)$$

$$r(l(t),t) = R(l(t))U(t) + p(l(t),t) \quad (19)$$

where $U(t) = [U_1(t), U_2(t)]^T$ and

$$R(l(t)) = 2\text{diag}(\sqrt{d_6(l(t))}d_{19}(l(t)), \sqrt{d_1(l(t))}d_{20}(l(t))),$$

$$Q(x) = \text{diag}\{Q_1(x), Q_2(x)\} = \text{diag}\{\sqrt{d_6(x)}, \sqrt{d_1(x)}\}.$$

$\bar{A}, C_3, \bar{B}$ are

$$\bar{A} = \begin{bmatrix} A_1 & d_{13}B_1C_2 \\ d_{17}B_1C_2 & A_2 \end{bmatrix}, C_3 = 2\begin{bmatrix} 0 & C_2 \\ C_2 & 0 \end{bmatrix}, \quad (20)$$

$$\bar{B} = \frac{1}{2}\begin{bmatrix} \frac{B_1d_{14}}{\sqrt{d_6(0)}} & \frac{B_1d_{12}}{\sqrt{d_1(0)}} \\ \frac{B_1d_{16}}{\sqrt{d_6(0)}} & \frac{B_1d_{18}}{\sqrt{d_1(0)}} \end{bmatrix} = \frac{1}{2}\begin{bmatrix} 0 & 0 \\ \frac{d_{14}}{\sqrt{d_6(0)}} & \frac{d_{12}}{\sqrt{d_1(0)}} \\ 0 & 0 \\ \frac{d_{16}}{\sqrt{d_6(0)}} & \frac{d_{18}}{\sqrt{d_1(0)}} \end{bmatrix} \quad (21)$$

where

$$A_1 = \begin{bmatrix} 0 & 1 \\ 0 & d_{11} \end{bmatrix}, A_2 = \begin{bmatrix} 0 & 1 \\ 0 & d_{15} \end{bmatrix}, B_1 = \begin{pmatrix} 0 \\ 1 \end{pmatrix}, C_2 = (\,0\;\;1\,).$$

$T_a(x) = \{T_{aij}(x)\}_{1\leq i,j\leq 2}$, $T_b(x) = \{T_{bij}(x)\}_{1\leq i,j\leq 2}$ are shown as follows

$$T_a(x) = \begin{bmatrix} s_1(x) + \frac{d_{10}(x)}{2} & \frac{d_7(x)}{2\sqrt{d_1(x)}} + \frac{d_9(x)}{2} \\ \frac{d_3(x)}{2\sqrt{d_6(x)}} + \frac{d_5(x)}{2} & s_2(x) + \frac{d_4(x)}{2} \end{bmatrix}, \quad (22)$$

$$T_b(x) = \begin{bmatrix} \frac{d_{10}(x)}{2} - s_1(x) & \frac{d_9(x)}{2} - \frac{d_7(x)}{2\sqrt{d_1(x)}} \\ \frac{d_5(x)}{2} - \frac{d_3(x)}{2\sqrt{d_6(x)}} & \frac{d_4(x)}{2} - s_2(x) \end{bmatrix}, \quad (23)$$

where $s_1(x) = \frac{d_8(x) - \frac{1}{2}d_6{}'(x)}{2\sqrt{d_6(x)}}$, $s_2(x) = \frac{d_2(x) - \frac{1}{2}d_1{}'(x)}{2\sqrt{d_1(x)}}$.

The following assumption is required by state estimation of ODE (18).

Assumption 5. $(\bar{A} - \bar{B}C_3, C_3)$ is observable .

Assumption 5 holds in the application of the DCV, which can be easily checked by the specific parameters of the DCV in the simulation.

3.2 Observer structure

The sensors only are placed at the actuated boundary and the available measurements are $u_t(l(t),t)$, $w_t(l(t),t)$, i.e., $p(l(t),t)$ being known through a convertor as

$$p(l(t),t) = [u_t(l(t),t) - \sqrt{d_6(l(t))}d_{19}(l(t))U_1(t), \; w_t(l(t),t) - \sqrt{d_1(l(t))}d_{20}(l(t))U_2(t)] \quad (24)$$

recalling (5)-(6), (12), (7) and (10).

Using the known signal $p(l(t),t)$, the observer for the coupled wave PDE plant (1)-(6) is constructed, which consists of two parts. The first part:

$$\hat{p}_t(x,t)+Q(x)\hat{p}_x(x,t)=T_a(x)\hat{r}(x,t)+T_b(x)\hat{p}(x,t)$$
$$+\Gamma_1(x,t)(p(l(t),t)-\hat{p}(l(t),t)), \quad (25)$$
$$\hat{r}_t(x,t)-Q(x)\hat{r}_x(x,t)=T_a(x)\hat{r}(x,t)+T_b(x)\hat{p}(x,t)$$
$$+\Gamma_2(x,t)(p(l(t),t)-\hat{p}(l(t),t)), \quad (26)$$
$$\hat{p}(0,t)=C_3\hat{W}(t)-\hat{r}(0,t), \quad (27)$$
$$\dot{\hat{W}}(t)=(\bar{A}-\bar{B}C_3)\hat{W}(t)+2\bar{B}\hat{r}(0,t)$$
$$+\Gamma_3(t)(p(l(t),t)-\hat{p}(l(t),t)), \quad (28)$$
$$\hat{r}(l(t),t)=R(l(t))U(t)+p(l(t),t) \quad (29)$$

where $\hat{p}=[\hat{y}(x,t),\hat{v}(x,t)]^T$, $\hat{r}=[\hat{k}(x,t),\hat{z}(x,t)]^T$, $\hat{W}(t)=[\hat{X}(t),\hat{Y}(t)]^T=[\hat{w}(0,t),\hat{w}_t(0,t),\hat{u}(0,t),\hat{u}_t(0,t)]^T$, and the second part:

$$\hat{w}_t(x,t)=\frac{1}{2}(\hat{z}(x,t)+\hat{v}(x,t)), \quad (30)$$
$$\hat{w}_x(x,t)=\frac{1}{2\sqrt{d_1(x)}}(\hat{z}(x,t)-\hat{v}(x,t)), \quad (31)$$
$$\hat{u}_t(x,t)=\frac{1}{2}(\hat{k}(x,t)+\hat{y}(x,t)), \quad (32)$$
$$\hat{u}_x(x,t)=\frac{1}{2\sqrt{d_6(x)}}(\hat{k}(x,t)-\hat{y}(x,t)). \quad (33)$$

Note:

1. (25)-(29) in the sense of a copy of plant (15)-(19) plus output injections is built to estimate the reformulated plant $p(x,t),r(x,t)$;

2. Once $p(x,t),r(x,t)$ are estimated successfully by (25)-(29), the estimations of the original plant are straightly obtained as (30)-(33) considering the transformations (7)-(14).

Next, the observer gains $\Gamma_1(x,t)$, $\Gamma_2(x,t)$ and $\Gamma_3(t)$ will be determined to achieve the exponential stability of the observer error system. A difference from the traditional ones should be noted that Γ_1, Γ_2 not only depend on the spatial variable x but also depends on time t because of the time-varying domain.

3.3 Observer error system

The observation problem is essentially to ensure the observer errors (differences between the estimated and real states) are reduced to zero, by choosing observer gains. Denote the observer errors as

$$\tilde{w}_t(x,t)=w_t(x,t)-\hat{w}_t(x,t), \quad (34)$$
$$\tilde{w}_x(x,t)=w_x(x,t)-\hat{w}_x(x,t), \quad (35)$$
$$\tilde{u}_t(x,t)=u_t(x,t)-\hat{u}_t(x,t), \quad (36)$$
$$\tilde{u}_x(x,t)=u_x(x,t)-\hat{u}_x(x,t), \quad (37)$$
$$\begin{aligned}\tilde{W}(x,t)&=W(x,t)-\hat{W}(t)\\&=[X(t),Y(t)]-[\hat{X}(t),\hat{Y}(t)]\\&=[w(0,t),w_t(0,t),u(0,t),u_t(0,t)]^T\\&\quad-[\hat{w}(0,t),\hat{w}_t(0,t),\hat{u}(0,t),\hat{u}_t(0,t)]^T\\&=[\tilde{X}(t),\tilde{Y}(t)]\\&=[\tilde{w}(0,t),\tilde{w}_t(0,t),\tilde{u}(0,t),\tilde{u}_t(0,t)]^T, \quad (38)\end{aligned}$$
$$\tilde{p}(x,t)=p(x,t)-\hat{p}(x,t)=[\tilde{y}(x,t),\tilde{v}(x,t)], \quad (39)$$
$$\tilde{r}(x,t)=r(x,t)-\hat{r}(x,t)=[\tilde{k}(x,t),\tilde{z}(x,t)]. \quad (40)$$

Recalling (15)-(19), (7)-(10) and (25)-(33), the resulting observer error dynamics is given by

$$\tilde{w}_t(x,t)=\frac{1}{2}(\tilde{z}(x,t)+\tilde{v}(x,t)), \quad (41)$$
$$\tilde{w}_x(x,t)=\frac{1}{2\sqrt{d_1(x)}}(\tilde{z}(x,t)-\tilde{v}(x,t)), \quad (42)$$
$$\tilde{u}_t(x,t)=\frac{1}{2}(\tilde{k}(x,t)+\tilde{y}(x,t)), \quad (43)$$
$$\tilde{u}_x(x,t)=\frac{1}{2\sqrt{d_6(x)}}(\tilde{k}(x,t)-\tilde{y}(x,t)), \quad (44)$$
$$\tilde{p}_t(x,t)+Q(x)\tilde{p}_x(x,t)=T_a(x)\tilde{r}(x,t)+T_b(x)\tilde{p}(x,t)$$
$$+\Gamma_1(x,t)\tilde{p}(l(t),t), \quad (45)$$
$$\tilde{r}_t(x,t)-Q(x)\tilde{r}_x(x,t)=T_a(x)\tilde{r}(x,t)+T_b(x)\tilde{p}(x,t)$$
$$+\Gamma_2(x,t)\tilde{p}(l(t),t), \quad (46)$$
$$\tilde{p}(0,t)=C_3\tilde{W}(t)-\tilde{r}(0,t), \quad (47)$$
$$\dot{\tilde{W}}(t)=(\bar{A}-\bar{B}C_3)\tilde{W}(t)+2\bar{B}\tilde{r}(0,t)+\Gamma_3(t)\tilde{p}(l(t),t), \quad (48)$$
$$\tilde{r}(l(t),t)=0, \quad (49)$$

where the subsystem (45)-(49) describing dynamics of the observer error of the system (15)-(19), determines the observer error of the plant (1)-(6) via (41)-(44). Therefore, the exponential stability of (45)-(49) is the core to make sure the proposed observer can be exponentially convergent to the actual states of the original plant (1)-(6).

3.4 Observer backtepping design

To find the observer gains $\Gamma_1(x,t),\Gamma_2(x,t),\Gamma_3(t)$ that guarantee that (45)-(49) is exponentially stable, we use a transformation to map (45)-(49) to a target observer error system whose exponential stability result is straightforward to obtain. The transformation is introduced as

$$\tilde{p}(x,t)=\tilde{\alpha}(x,t)-\int_x^{l(t)}\bar{\varphi}(x,y)\tilde{\alpha}(y,t)dy, \quad (50)$$
$$\tilde{r}(x,t)=\tilde{\beta}(x,t)-\int_x^{l(t)}\bar{\psi}(x,y)\tilde{\alpha}(y,t)dy, \quad (51)$$
$$\tilde{W}(t)=\tilde{S}(t)+\int_0^{l(t)}\bar{K}(y)\tilde{\alpha}(y,t)dy, \quad (52)$$

where kernels $\bar{\varphi}(x,y)=\{\varphi_{ij}(x,y)\}_{1\le i,j\le 2}$, $\bar{\psi}(x,y)=\{\psi_{ij}(x,y)\}_{1\le i,j\le 2}$ on a triangular domain $\mathscr{D}_1=\{0\le x\le y\le l(t)\}$ and $\bar{K}(y)=\{\bar{K}_{ij}(y)\}_{1\le i\le 4,1\le j\le 2}$ are to be determined.

The target observer error system is set up as

$$\tilde{\alpha}_t(x,t)+Q(x)\tilde{\alpha}_x(x,t)=T_a(x)\tilde{\beta}(x,t)+\bar{T}_b(x)\tilde{\alpha}(x,t)$$
$$+\int_x^{l(t)}\bar{M}(x,y)\tilde{\beta}(y,t)dy, \quad (53)$$
$$\tilde{\beta}_t(x,t)-Q(x)\tilde{\beta}_x(x,t)=\int_x^{l(t)}\bar{N}(x,y)\tilde{\beta}(y,t)dy$$
$$+T_a(x)\tilde{\beta}(x,t), \quad (54)$$
$$\tilde{\alpha}(0,t)=C_3\tilde{S}(t)-\tilde{\beta}(0,t)+\int_0^{l(t)}H(y)\tilde{\alpha}(y,t)dy, \quad (55)$$
$$\tilde{\beta}(l(t),t)=0, \quad (56)$$
$$\dot{\tilde{S}}(t)=\check{A}\tilde{S}(t)+\check{E}\tilde{\beta}(0,t)+\int_0^{l(t)}G(y)\tilde{\beta}(y,t)dy \quad (57)$$

where $\check{A}=\bar{A}-\bar{B}C_3-L_0C_3$ is a Hurwitz matrix by choosing $L_0=\{L_{0ij}\}_{1\le i\le 4,1\le j\le 2}$ recalling Assumption 5, and $\bar{M}(x,y)$, $\bar{N}(x,y)$ satisfy

$$\bar{M}(x,y)=\int_x^y \bar{\varphi}(x,z)\bar{M}(z,y)dz+\bar{\varphi}(x,y)T_a(y), \tag{58}$$

$$\bar{N}(x,y)=\int_x^y \bar{\psi}(x,z)\bar{M}(z,y)dz+\bar{\psi}(x,y)T_a(y). \tag{59}$$

Note that $H(y)=\{h_{ij}(y)\}_{1\le i,j\le 2}$ in (55) is a strict lower triangular matrix as

$$H(y)=\begin{pmatrix} 0 & 0 \\ \bar{\psi}_{2,1}(0,y)+\bar{\varphi}_{2,1}(0,y)+\bar{K}_{21}(y) & 0 \end{pmatrix}, \tag{60}$$

and $G(y)=\{G_{ij}(y)\}_{1\le i\le 4,1\le j\le 2}, \check{E}=\{\check{E}_{ij}\}_{1\le i\le 4,1\le j\le 2}$ in (57) are equal to $-\bar{K}(0,y)\bar{T}_a(y)-\int_0^y \bar{K}(0,z)\bar{M}(z,y)dz$ and $L_0+2\bar{B}$ respectively. The exponential stability of the target system (53)-(57) will be seen in Lemma 2.

By matching (45)-(49) and (53)-(57) through the transformation (50)-(52), the conditions on the kernels in (50)-(52) and observer gains in (25), (26), (28) are obtained as follows. Kernels $\bar{\varphi}(x,y)$, $\bar{\psi}(x,y)$, $\bar{K}(y)$ should satisfy the matrix equations:

$$\begin{aligned}
&-\bar{\varphi}_y(x,y)Q(y)-Q(x)\bar{\varphi}_x(x,y)-\bar{\varphi}(x,y)Q'(y)\\
&+T_a(x)\bar{\psi}(x,y)+T_b(x)\bar{\varphi}(x,y)-\bar{\varphi}(x,y)\bar{T}_b(y)=0, &(61)\\
&-\bar{\psi}_y(x,y)Q(y)+Q(x)\bar{\psi}_x(x,y)-\bar{\psi}(x,y)Q'(y)\\
&+T_a(x)\bar{\psi}(x,y)-\bar{\psi}(x,y)\bar{T}_b(y)+T_b(x)\bar{\varphi}(x,y)=0, &(62)\\
&Q(x)\bar{\varphi}(x,x)-\bar{\varphi}(x,x)Q(x)=T_b(x)-\bar{T}_b(x), &(63)\\
&Q(x)\bar{\psi}(x,x)+\bar{\psi}(x,x)Q(x)=-T_b(x), &(64)\\
&\bar{\psi}(0,y)+\bar{\varphi}(0,y)+C_3\bar{K}(y)=H(y), &(65)\\
&-\bar{K}'(y)Q(y)+(\bar{A}-\bar{B}C_3-L_0C_3)\bar{K}(y)-\bar{K}(y)[Q'(y)+\bar{T}_b(y)]\\
&-L_0\bar{\varphi}(0,y)-(2\bar{B}+L_0)\bar{\psi}(0,y)=0, &(66)\\
&\bar{K}(0)=L_0Q(0)^{-1} &(67)
\end{aligned}$$

and the observe gains are obtained as

$$\Gamma_1(x,t)=\dot{l}(t)\bar{\varphi}(x,l(t))-\bar{\varphi}(x,l(t))Q(l(t)), \tag{68}$$

$$\Gamma_2(x,t)=\dot{l}(t)\bar{\psi}(x,l(t))-\bar{\psi}(x,l(t))Q(l(t)), \tag{69}$$

$$\Gamma_3(t)=\dot{l}(t)\bar{K}(l(t))-\bar{K}(l(t))Q(l(t)). \tag{70}$$

Lemma 1. After adding an additional artificial boundary condition for the element $\bar{\varphi}_{21}$ in the matrix $\bar{\varphi}$, the matrix equations (61)-(67) have a unique solution $\bar{\varphi},\bar{\psi}\in L^\infty(\mathscr{D}_1)$, $\bar{K}\in L^\infty([0,l(t)])$.

Proof. Please see Wang et al. (2019a) for the proof.

Following similar steps as above, the inverse transformation of (50)-(52) can be determined as

$$\tilde{\alpha}(x,t)=\tilde{p}(x,t)-\int_x^{l(t)}\check{\varphi}(x,y)\tilde{p}(y,t)dy, \tag{71}$$

$$\tilde{\beta}(x,t)=\tilde{r}(x,t)-\int_x^{l(t)}\check{\psi}(x,y)\tilde{p}(y,t)dy, \tag{72}$$

$$\tilde{S}(t)=\tilde{W}(t)+\int_0^{l(t)}\check{K}(y)\tilde{r}(y,t)dy, \tag{73}$$

where $\check{\varphi}(x,y)\in R^{2\times 2}$, $\check{\psi}(x,y)\in R^{2\times 2}$ and $\check{K}(y)\in R^{4\times 2}$ are kernels on $\mathscr{D}_1$ and $0\le y\le l(t)$, respectively.

4. STABILITY ANALYSIS OF OBSERVER ERROR SYSTEM

Before showing the performance of the proposed observer on tracking the actual states in the original plant (1)-(6) in the next theorem, the stability result of the observer error subsystem (45)-(49) which dominates the observer errors of the original plant (1)-(6) is given in the following lemma.

Lemma 2. Consider the observer error subsystem (45)-(49), there exist positive constants Υ_3,σ_3 such that

$$\begin{aligned}
&\left(\|\tilde{p}(\cdot,t)\|^2+\|\tilde{r}(\cdot,t)\|^2+\left|\tilde{W}(t)\right|^2\right)^{\frac{1}{2}}\\
&\le\Upsilon_3\left(\|\tilde{p}(\cdot,0)\|^2+\|\tilde{r}(\cdot,0)\|^2+\left|\tilde{W}(0)\right|^2\right)^{\frac{1}{2}}e^{-\sigma_3 t}.
\end{aligned} \tag{74}$$

Proof. Expanding (53)-(57) as $\tilde{\alpha}=[\tilde{\alpha}_1,\tilde{\alpha}_2]^T$, $\tilde{\beta}=[\tilde{\beta}_1,\tilde{\beta}_2]^T$, one obtains

$$\begin{aligned}
&\tilde{\alpha}_{it}(x,t)+Q_i(x)\tilde{\alpha}_{ix}(x,t)=\sum_{j=1}^{2}T_{aij}(x)\tilde{\beta}_j(x,t)\\
&+\bar{T}_{bi}(x)\tilde{\alpha}_i(x,t)+\int_x^{l(t)}\sum_{j=1}^{2}\bar{M}_{ij}(x,y)\tilde{\beta}_j(y,t)dy, &(75)\\
&\tilde{\beta}_{it}(x,t)-Q_i(x)\tilde{\beta}_{ix}(x,t)=\int_x^{l(t)}\sum_{j=1}^{2}\bar{N}_{ij}(x,y)\tilde{\beta}_j(y,t)dy\\
&+\sum_{j=1}^{2}T_{aij}(x)\tilde{\beta}_j(x,t), &(76)\\
&\tilde{\alpha}_i(0,t)=C_3\tilde{S}(t)-\tilde{\beta}_i(0,t)+(i-1)\int_0^{l(t)}h_{21}(y)\tilde{\alpha}_1(y,t)dy, &(77)\\
&\tilde{\beta}_i(l(t),t)=0 &(78)
\end{aligned}$$

for $i=1,2$, and $\tilde{S}(t)$ is governed by

$$\begin{aligned}
\dot{\tilde{S}}(t)=&\check{A}\tilde{S}(t)+\check{E}[\tilde{\beta}_1(0,t),\tilde{\beta}_2(0,t)]^T\\
&+\int_0^{l(t)}G(y)[\tilde{\beta}_1(y,t),\tilde{\beta}_2(y,t)]^T dy.
\end{aligned} \tag{79}$$

In (75)-(79), $\tilde{\beta}_i(\cdot,t)$ are independent and $\tilde{\beta}_i(\cdot,t)=0$ is achieved in a finite time because of (78). Thus $\tilde{S}(t)$ is exponentially convergent to zero because $\check{A}$ is Hurwitz. $\tilde{\beta}_{1,2}(\cdot,t)$ flow into $\tilde{\alpha}_1(\cdot,t)$, $\tilde{\alpha}_2(\cdot,t)$ subsystems. $\tilde{\alpha}_1(\cdot,t)$ are exponentially convergent to zero because of the exponential convergence of $\tilde{\alpha}_1(0,t)$ considering (77) for $i=1$. $\tilde{\alpha}_1(\cdot,t)$ flow into $\tilde{\alpha}_2(0,t)$ through the boundary (77), where exponential convergence of $\tilde{\alpha}_2(0,t)$ also can be obtained for $i=2$ because all signals at the right hand side of the equal sign are exponentially convergent to zero. It follows that $\tilde{\alpha}_2(\cdot,t)$ are exponentially convergent to zero as well.

The exponential stability result would be seen more clearly by using the following Lyapunov function as

$$\begin{aligned}
V_e(t)=&\frac{\check{r}_{b1}}{2}\int_0^{l(t)}e^{-\check{\delta}_1 x}\tilde{\alpha}_1(x,t)^T Q_1(x)^{-1}\tilde{\alpha}_1(x,t)dx\\
&+\frac{\check{r}_{a1}}{2}\int_0^{l(t)}e^{\check{\delta}_2 x}\tilde{\beta}_1(x,t)^T Q_1(x)^{-1}\tilde{\beta}_1(x,t)dx\\
&+\frac{\check{r}_{a2}}{2}\int_0^{l(t)}e^{\check{\delta}_2 x}\tilde{\beta}_2(x,t)^T Q_2(x)^{-1}\tilde{\beta}_2(x,t)dx+\tilde{S}(t)^T P_2\tilde{S}(t)\\
&+\frac{\check{r}_{b2}}{2}\int_0^{l(t)}e^{-\check{\delta}_1 x}\tilde{\alpha}_2(x,t)^T Q_2(x)^{-1}\tilde{\alpha}_2(x,t)dx,
\end{aligned} \tag{80}$$

where a positive definite matrix $P_2=P_2^T$ is the solution to the Lyapunov equation $P_2\check{A}+\check{A}^T P_2=-\hat{Q}_2$, for some $\hat{Q}_2=\hat{Q}_2^T>0$, and $\check{r}_{a1},\check{r}_{a2},\check{r}_{b1},\check{r}_{b2},\check{\delta}_1,\check{\delta}_2$ are positive constants. The following inequality holds

$$\mu_{e1}\Omega_e(t)\le V_e(t)\le\mu_{e2}\Omega_e(t) \tag{81}$$

for some positive μ_{e1}, μ_{e2}, where $\Omega_e(t) = \|\tilde{\alpha}(\cdot,t)\|^2 + \|\tilde{\beta}(\cdot,t)\|^2 + |\tilde{S}(t)|^2$. Note that $\|\tilde{\alpha}(\cdot,t)\|^2 = \int_0^{l(t)} \tilde{\alpha}_1(\cdot,t)^2 dx + \int_0^{l(t)} \tilde{\alpha}_2(\cdot,t)^2 dx$.

Taking the derivative of (80) along (75)-(79), choosing appropriate $\check{r}_{a1}, \check{r}_{a2}$, $\check{r}_{b1}, \check{r}_{b2}$, $\check{\delta}_1, \check{\delta}_2$, of which the detailed process is shown in Wang et al. (2019a), we can obtain

$$\dot{V}_e(t) \leq -\eta_e V_e(t) \tag{82}$$

for some positive η_e which is associated with L_0. It follows that the exponential stability result in the sense of

$$\begin{aligned}&\left(\|\tilde{\alpha}(x,t)\|^2 + \|\tilde{\beta}(x,t)\|^2 + |\tilde{S}(t)|^2\right)^{\frac{1}{2}} \\ \leq &\xi_e \left(\|\tilde{\alpha}(x,0)\|^2 + \|\tilde{\beta}(x,0)\|^2 + |\tilde{S}(0)|^2\right)^{\frac{1}{2}} e^{-\eta_e t},\end{aligned} \tag{83}$$

for some positive ξ_e and η_e.

Recalling the direct and inverse backstepping transformations (50)-(52), (71)-(73), and applying Cauchy-Schwarz inequality, the proof of Lemma 2 is completed.

Applying the exponential stability result of the observer error subsystem (45)-(49) in Lemma 2 and recalling the relationships (41)-(44), we obtain the following theorem about the performance of the observer on tracking the actual states in the original plant (1)-(6).

Theorem 1. Considering the observer error system (41)-(49) with the observer gains $\Gamma_1(x,t)$ (68), $\Gamma_2(x,t)$ (69), $\Gamma_3(t)$ (70), for any initial data $(\tilde{u}(x,0), \tilde{u}_t(x,0)) \in H^2(0,L) \times H^1(0,L)$, $(\tilde{w}(x,0), \tilde{w}_t(x,0)) \in H^2(0,L) \times H^1(0,L)$, there exist positive constants Υ_4, σ_4 such that

$$\Phi_4(t) \leq \Upsilon_4 \Phi_4(0) e^{-\sigma_4 t},$$

where $\Phi_4(t) = (\|\tilde{u}_t(\cdot,t)\|^2 + \|\tilde{u}_x(\cdot,t)\|^2 + \|\tilde{w}_t(\cdot,t)\|^2 + \|\tilde{w}_x(\cdot,t)\|^2 + \tilde{w}(0,t)^2 + \tilde{w}_t(0,t)^2 + \tilde{u}(0,t)^2 + \tilde{u}_t(0,t)^2)^{\frac{1}{2}}$. It means the observer states in (25)-(33) can be exponentially convergent to the actual values in (1)-(6) according to (34)-(37).

Proof. Recalling Lemma 2 and (38)-(40), the following inequality holds

$$\Phi_{4a}(t) \leq \Upsilon_{4a} \Phi_{4a}(0) e^{-\sigma_{4a} t},$$

where

$$\begin{aligned}\Phi_{4a}(t) = &\big(\|\tilde{y}(\cdot,t)\|^2 + \|\tilde{v}(\cdot,t)\|^2 + \|\tilde{k}(\cdot,t)\|^2 + \|\tilde{z}(\cdot,t)\|^2 \\ &+ \left|\tilde{X}(t)\right|^2 + \left|\tilde{Y}(t)\right|^2\big)^{\frac{1}{2}}\end{aligned}$$

for some positive constants $\Upsilon_{4a}, \sigma_{4a}$.

According to (41)-(44), of which the inverse transformation where $\tilde{u}_t(\cdot,t), \tilde{u}_x(\cdot,t)$, $\tilde{w}_t(\cdot,t), \tilde{w}_x(\cdot,t)$ are represented by $\tilde{z}(\cdot,t), \tilde{v}(\cdot,t), \tilde{k}(\cdot,t), \tilde{y}(\cdot,t)$ is straightforward to obtain, the proof of Theorem 1 is then completed recalling (38).

5. SIMULATION TEST ON VIBRATION ESTIMATION OF DCV

The two-dimensional vibration dynamics of DCV Wang et al. (2019a) is a specific case of the general plant (1)-(6) with setting the coefficients as

$$d_1(x) = \frac{\frac{3}{2} EA_a \bar{\phi}(x)^2 + T(x)}{m_c}, \tag{84}$$

$$d_2(x) = \frac{EA_a \bar{\varepsilon}'(x) + \rho g}{m_c},\ d_3 = \frac{-EA_a \bar{\phi}'(x)}{m_c}, \tag{85}$$

$$d_4 = \frac{-c_v}{m_c},\ d_5 = 0,\ d_6 = \frac{EA_a}{m_c},\ d_7(x) = \frac{-EA_a \bar{\phi}'(x)}{m_c}, \tag{86}$$

Table 1. Physical parameters of the DSV.

Parameters (units)	values
Final cable length L (m)	1210
Initial cable length $l(0)$ (m)	250
Maximum descending velocity $\bar{M}$ (m/s)	10
Operation time t_f (s)	120
Cable cross-sectional area A_a (m^2)	0.47×10^{-3}
Cable effective Youngs Modulus E (N/m^2)	7.03×10^{10}
Cable linear density m_c (kg/m)	8. 95
Payload mass M_L (kg)	8000
Payload volume V_p (m^3)	5
Gravitational acceleration g (m/s^2)	9.8
Drag coefficient C_d	1
Stream velocity V_s (m/s)	2
Seawater density ρ_w (kgm^{-3})	1024
Longitudinal damping coefficient in cable c_u	0.5
Lateral damping coefficient in cable c_v	0.3
Longitudinal damping coefficient at attached payload c_h	0.5
Lateral damping coefficient at attached payload c_w	0.3

$$d_8 = d_9 = 0,\ d_{10} = \frac{-c_u}{m_c},\ d_{11} = \frac{-c_w}{M_L},\ d_{12} = \frac{-EA_a \bar{\phi}(0)^2}{2M_L}, \tag{87}$$

$$d_{13} = 0,\ d_{14} = \frac{-EA_a \bar{\phi}(0)}{M_L},\ d_{15} = \frac{-c_h}{M_L}, d_{16} = \frac{-EA_a}{M_L}, \tag{88}$$

$$d_{17} = 0,\ d_{18} = \frac{EA_a \bar{\phi}(0)}{2M_L},\ d_{19} = \frac{1}{EA_a}, \tag{89}$$

$$d_{20}(l(t)) = \frac{1}{EA_a \bar{\varepsilon}(l(t)) + \frac{EA_a}{2} \bar{\phi}(l(t))^2 + T(l(t))}, \tag{90}$$

where $T(x)$, $\bar{\varepsilon}(x)$ and $\bar{\phi}(x)$ are

$$T(x) = \rho g x + Mg,\ \ \bar{\varepsilon}(x) = \frac{1}{EA_a}\sqrt{(\rho g x + Mg)^2 + F_0^2},$$

$$\bar{\phi}(x) = \bar{\vartheta}(x) - \theta = \arctan\left(\frac{F_0}{\rho g x + Mg}\right) - \theta,$$

$F_0 = \frac{\rho_w}{2} C_d V_s^2$ being the water-stream caused drag force Bohm et al. (2014), $\rho = m_c - \rho_w A_a$, $M = M_L - \rho_w V_p$ considering the effect of buoyancy, and the angles $\bar{\phi}(x), \theta, \bar{\vartheta}(x)$ being shown in Fig. 1. The values of the physical parameters are shown in Table 1. x in (84)-(90) can be represented by ι via (91). Note that the time-varying domain plant with pre-determined time-varying functions $l(t)$ and $\dot{l}(t)$ shown in Fig. 2, is converted to the one on the fixed domain $\iota = [0,1]$ with time-varying coefficients related to $l(t), \dot{l}(t), \ddot{l}(t)$ via introducing

$$\iota = \frac{x}{l(t)}, \tag{91}$$

i.e., representing $u(x,t)$ by $u(\iota,t)$ as

$$u_x(x,t) = \frac{1}{l(t)} u_\iota(\iota,t),\ u_{xx}(x,t) = \frac{1}{l(t)^2} u_{\iota\iota}(\iota,t), \tag{92}$$

$$u_t(x,t) = u_t(\iota,t) - \frac{\dot{l}(t)\iota}{l(t)} u_\iota(\iota,t), \tag{93}$$

$$\begin{aligned}u_{tt}(x,t) = &u_{tt}(\iota,t) - \frac{2\dot{l}(t)\iota}{l(t)} u_{\iota t}(\iota,t) - \frac{\dot{l}(t)^2 \iota^2}{l(t)^2} u_{\iota\iota}(\iota,t) \\ &- \frac{(l(t)\ddot{l}(t) - 2\ddot{l}(t)^2)\iota}{l(t)^2} u_\iota(\iota,t),\end{aligned} \tag{94}$$

and then the simulation is conducted using the finite difference method with time step and space step as 0.001 and 0.05 respectively. The initial conditions of the plant are defined according to the steady state, as $u_x(\cdot,0) = \bar{\varepsilon}(\cdot)$, $u_t(\cdot,0) = 0$ and $w_x(\cdot,0) = -\bar{\phi}(\cdot)$, $w_t(\cdot,0) = 0$. With defining $u(0,0) = 0$ and $w(l(0),0) =$

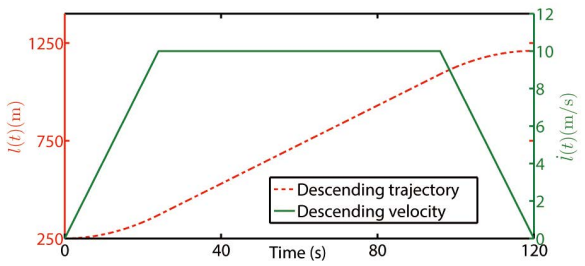

Fig. 2. Descending trajectory and velocity, i.e., the time-varying cable length $l(t)$ and the changing rate $\dot{l}(t)$.

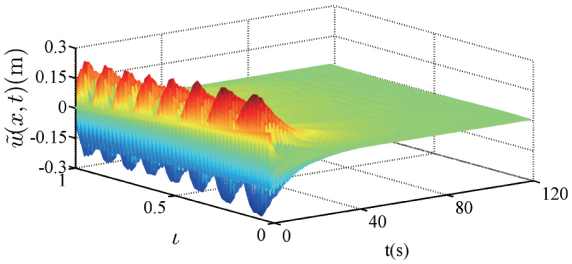

Fig. 3. Observer error of lateral vibrations $\tilde{w}(x,t)$.

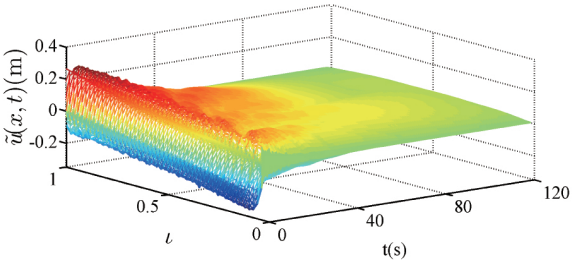

Fig. 4. Observer error of longitudinal vibrations $\tilde{u}(x,t)$.

0. All initial conditions $\hat{k}(\cdot,0),\hat{y}(\cdot,0),\hat{z}(\cdot,0),\hat{v}(\cdot,0),\hat{W}(0)$ of the observer (25)-(33) are set as zero. The performance of the observer on tracking the actual states can be seen in Figs. 3-4, which show the observer errors of both lateral and longitudinal vibrations are convergent to zero. Note that the following equations are used to obtain $\hat{u},\hat{w}$ from $\hat{k},\hat{y},\hat{z},\hat{v}$, $\hat{u}(\iota,t) = \int_0^\iota \frac{1}{2\sqrt{d_6(\varsigma)}}(\hat{k}(\varsigma,t)-\hat{y}(\varsigma,t))d\varsigma + \bar{C}_1\hat{W}(t)$, $\hat{w}(\iota,t) = \int_0^\iota \frac{1}{2\sqrt{d_1(\varsigma)}}(\hat{z}(\varsigma,t)-\hat{v}(\varsigma,t))d\varsigma + \bar{C}_2\hat{W}(t)$, according to (30)-(33) and (38), where $\bar{C}_1 = [0,0,1,0]$ and $\bar{C}_2 = [1,0,0,0]$.

6. CONCLUSION AND FUTURE WORK

This work is motivated by estimation of longitudinal-lateral coupled vibrations of a deep-sea construction vessel of which the dynamics is described by a 4×4 coupled heterodirectional hyperbolic PDE-ODE system characterized by spatially-varying coefficients and on a time-varying domain. The observer designs are conducted via the backstepping method and the exponential stability result of the observer error system is proved by Lyapunov analysis. The simulation verifies that the proposed vibration observer can effectively estimate the longitudinal-lateral vibrations in DCV.

REFERENCES

O. M. Aamo, "Disturbance rejection in 2×2 linear hyperbolic systems", *IEEE Trans. Autom. Control*, 58(5), pp.1095-1106, 2013.

H. Anfinsen and O. M. Aamo, "Disturbance rejection in general heterodirectional 1-D linear hyperbolic systems using collocated sensing and control", *Automatica*, 76, pp.230-242, 2017a.

H. Anfinsen and O. M. Aamo, " Adaptive output-feedback stabilization of linear 2×2 hyperbolic systems using anti-collocated sensing and control", *Systems & Control Letters*, 104, pp.86-94, 2017b.

M. Bohm, M. Krstic, S. Kuchler and O. Sawodny, "Modeling and boundary control of a hanging cable immersed in water", *Journal of Dynamic Systems, Measurement, and Control*,136, pp. 011006, 2014.

J. Deutscher, "Finite-time output regulation for linear 2×2 hyperbolic systems using backstepping". *Automatica*, 75, pp.54-62, 2017a.

J. Deutscher, "Output regulation for general linear heterodirectional hyperbolic systems with spatially-varying coefficients". *Automatica*, 85, pp.34-42, 2017b.

J. Deutscher, N. Gehring and R. Kern "Output feedback control of general linear heterodirectional hyperbolic PDE-ODE systems with spatially-varying coefficients", *Int. J. Control*, 92, pp.2274-2290, 2019.

B. How, S.S. Ge and Y. S. Choo "Control of Coupled Vessel, Crane, Cable, and Payload Dynamics for Subsea Installation Operations". *IEEE Transactions on Control Systems Technology* 19, pp. 208-220, 2011.

L. Hu, F. Di Meglio, R. Vazquez and M. Krstic, "Control of homodirectional and general heterodirectional linear coupled hyperbolic PDEs", *IEEE Trans. Autom. Control*, 61(11), pp.3301-3314, 2016.

F. Di Meglio, F. Bribiesca, L. Hu and M. Krstic, "Stabilization of coupled linear heterodirectional hyperbolic PDE-ODE systems", *Automatica*, 87, pp.281-289, 2018.

C. Roman, D. Bresch-Pietri, C. Prieur and O. Sename, "Robustness to in-domain viscous damping of a collocated boundary adaptive feedback law for an anti-damped boundary wave PDE", *IEEE Trans. Autom. Control*, 64(8), pp.3284-3299, 2019.

T. Stensgaard, C. White and K. Schiffer, "Subsea Hardware Installation from a FDPSO". In Offshore Technology Conference, 2010.

R.G. Standing, B.G. Mackenzie and R.O. Snell, "Enhancing the technology for deepwater installation of subsea hardware". In Offshore Technology Conference,2002.

J. Wang and M. Krstic, "Vibration suppression for coupled wave PDEs in deep-sea construction", avaliable on Arxiv,2019a.

J. Wang, S.-X. Tang and M. Krstic, "Adaptive output-feedback control of torsional vibration in off-shore rotary oil drilling systems", *Automatica*,10.1016/j.automatica.2019.108640,2020.

J. Wang, S. Koga, Y. Pi and M. Krstic, "Axial vibration suppression in a PDE Model of ascending mining cable elevator", *J. Dyn. Sys., Meas., Control.*, 140, pp. 111003, 2018a.

J. Wang, Y. Pi and M. Krstic, "Balancing and suppression of oscillations of tension and cage in dual-cable mining elevators", *Automatica*, 98, pp. 223-238, 2018b.